The Astrophysical Journal, 783:71 (6pp), 2014 March 10 doi:10.1088/0004-637X/783/2/71

KARL G. JANSKY VERY LARGE ARRAY OBSERVATIONS OF COLD DUST AND MOLECULAR GAS IN STARBURSTING QUASAR HOST GALAXIES AT $z \sim 4.5$

J. Wagg[1,2,3], C. L. Carilli[2,4], M. Aravena[3,5], P. Cox[6], L. Lentati[2], R. Maiolino[2], R. G. McMahon[7], D. Riechers[8], F. Walter[9], P. Andreani[10], R. Hills[2], and A. Wolfe[11]
[1] Square Kilometre Array Organisation, Lower Withington, Cheshire, UK; j.wagg@skatelescope.org
[2] Cavendish Laboratory, University of Cambridge, Cambridge, UK
[3] European Southern Observatory, Casilla 19001, Santiago, Chile
[4] National Radio Astronomy Observatory, Socorro, NM, USA
[5] Núcleo de Astronomía, Facultad de Ingeniería, Universidad Diego Portales, Av. Ejército 441, Santiago, Chile
[6] Joint ALMA Observatory, Santiago, Chile
[7] Institute of Astronomy, University of Cambridge, Cambridge, UK
[8] Cornell University, Ithaca, NY, USA
[9] Max-Planck Institute for Astronomy, Heidelberg, Germany
[10] European Southern Observatory, Garching, Germany
[11] Department of Physics and Center for Astrophysics and Space Sciences, UCSD, La Jolla, CA, USA
Received 2013 November 4; accepted 2013 December 26; published 2014 February 18

ABSTRACT

We present Karl G. Jansky Very Large Array (VLA) observations of 44 GHz continuum and CO $J = 2$–1 line emission in BRI 1202−0725 at $z = 4.7$ (a starburst galaxy and quasar pair) and BRI 1335−0417 at $z = 4.4$ (also hosting a quasar). With the full 8 GHz bandwidth capabilities of the upgraded VLA, we study the (rest-frame) 250 GHz thermal dust continuum emission for the first time along with the cold molecular gas traced by the low-J CO line emission. The measured CO $J = 2$–1 line luminosities of BRI 1202−0725 are $L'_{\rm CO} = (8.7 \pm 0.8) \times 10^{10}$ K km s^{-1} pc^2 and $L'_{\rm CO} = (6.0 \pm 0.5) \times 10^{10}$ K km s^{-1} pc^2 for the submillimeter galaxy (SMG) and quasar, respectively, which are equal to previous measurements of the CO $J = 5$–4 line luminosities implying thermalized line emission, and we estimate a combined cold molecular gas mass of $\sim 9 \times 10^{10}\ M_\odot$. In BRI 1335−0417 we measure $L'_{\rm CO} = (7.3 \pm 0.6) \times 10^{10}$ K km s^{-1} pc^2. We detect continuum emission in the SMG BRI 1202−0725 North ($S_{44\,\rm GHz} = 51 \pm 6\,\mu$Jy), while the quasar is detected with $S_{44\,\rm GHz} = 24 \pm 6\,\mu$Jy and in BRI 1335−0417 we measure $S_{44\,\rm GHz} = 40 \pm 7\,\mu$Jy. Combining our continuum observations with previous data at (rest-frame) far-infrared and centimeter wavelengths, we fit three-component models in order to estimate the star formation rates. This spectral energy distribution fitting suggests that the dominant contribution to the observed 44 GHz continuum is thermal dust emission, while either thermal free–free or synchrotron emission contributes less than 30%.

Key words: cosmology: observations – early universe – galaxies: evolution – galaxies: formation – galaxies: high-redshift – galaxies: starburst

Online-only material: color figures

1. INTRODUCTION

The high-redshift formation of some of the most massive present-day galaxies is often accompanied by episodes of extreme far-infrared (FIR) luminosity, as highlighted by the phenomena of submillimeter/millimeter bright quasar host galaxies and starbursting submillimeter galaxies (SMGs). The interpretation of dust-heated star formation to explain the rest-frame FIR continuum properties of these populations is supported by the detection of redshifted [C II] line emission (e.g., Maiolino et al. 2005; Stacey et al. 2010; Venemans et al. 2012; Wang et al. 2013), as this is typically the strongest cooling line in the FIR spectrum of nearby galaxies (e.g., Stacey et al. 1991). Fueling the star formation and active galactic nucleus (AGN) activity requires significant molecular gas reservoirs, most efficiently studied through observations of redshifted CO line emission (see Carilli & Walter 2013 for a recent review). Together, these line and continuum observations can probe the physical conditions and kinematic properties of the interstellar medium in galaxies over much of the history of the universe.

Recent studies of gas and dust in high-redshift galaxies have used photoionization models along with measured values of the relative intensity between the FIR continuum, low-J CO, and [C II] line emission to constrain the ionization rate and density of the interstellar medium (e.g., Stacey et al. 2010; Ivison et al. 2010). With new facilities like the Atacama Large Millimeter/submillimeter Array (ALMA) and the upgraded Very Large Array (VLA) it is now possible to perform similar analyses at kpc-scale resolution with some of the most distant starburst galaxies and AGNs, while also constraining their kinematic properties (e.g., Riechers et al. 2011; Ivison et al. 2011; Wang et al. 2013; Carilli et al. 2013). Furthermore, with the combined continuum sensitivity of these interferometers, one can constrain the emissivity of the thermal dust continuum emission and obtain independent estimates of the star formation rates (SFRs) through detection of thermal free–free emission.

The FIR-luminous quasar host galaxies, BRI 1335−0417 and BRI 1202−0725, are two well-studied cases of massive, unlensed galaxy formation roughly 1.5 Gyr after the big bang. BRI 1335−0417 is believed to be a "wet" merger at $z = 4.4$ with an estimated FIR luminosity of $L_{\rm FIR} \sim 3 \times 10^{13}\ L_\odot$ fueled by $\sim 9 \times 10^{10}\ M_\odot$ of cold molecular gas traced by CO line emission (Storrie-Lombardi et al. 1996; Ohta et al. 1996; Guilloteau et al. 1997; Benford et al. 1999; Carilli et al. 1999, 2002; Riechers et al. 2008). Similarly, BRI 1202−0725 at $z = 4.7$ is a quasar host galaxy discovered in the Automated Photographic Measuring survey (Irwin et al. 1991) and has been shown to be composed of two FIR-luminous radio sources separated by $\sim 3\farcs8$

(Omont et al. 1996; Yun et al. 2000). Both the quasar host galaxy BRI 1202−0725 South and the optically faint SMG companion to the north have FIR luminosities in excess of $10^{13}\ L_{\odot}$ and a combined cold molecular gas mass of $\sim 10^{11}\ M_{\odot}$ (Carilli et al. 2002; Iono et al. 2006; Riechers et al. 2006). Within the same region, Hu et al. (1996) identified two fainter Lyα companions, both of which are thought to exhibit faint 157.7 μm [C II] line emission (Carilli et al. 2013). Submillimeter interferometric observations of [C II] and dust continuum emission with ALMA show that the Lyα companion to the SW of the quasar is also luminous in the FIR (Wagg et al. 2012; R. Williams et al., in preparation). It is likely that BRI 1202−0725 is at an early stage of a merger between multiple gas-rich systems (Salomé et al. 2012).

In this work we present VLA observations of rest-frame 250 GHz continuum and redshifted CO $J = 2$–1 line emission in the quasar host galaxies, BRI 1202−0725 and BRI 1335−0417. We adopt a cosmological model with $(\Omega_{\Lambda}, \Omega_m, h) = (0.73, 0.27, 0.71)$ (Spergel et al. 2007).

2. OBSERVATIONS AND DATA REDUCTION

Observations were carried out with 27 elements of the VLA on four dates in January and February of 2013, while the array was in the most compact D-configuration. The rest frequency of the CO $J = 2$–1 line is 230.538 GHz, so that at the redshifts of our targets this line can be observed at ∼40.5 GHz for the two most luminous galaxies in the BRI 1202−0725 system, and at 42.6 GHz in BRI 1335−0417. Each field was observed for a total of 8 hr including overheads associated with complex gain, bandpass, and flux density calibration. In the case of each target field, 3C 286 was used to calibrate the flux density and bandpass shape, while J1229+0203 and J1354−0206 were used to calibrate the complex gains for BRI 1202−0725 and BRI 1335−0417, respectively. Using the recently commissioned 8 GHz bandwidth correlator mode with the *Q*-band receivers, our observations covered 40–48 GHz with a spectral resolution of 2 MHz. The frequency coverage in this mode is not contiguous, and small 8 MHz gaps between subbands mean that two slightly offset tunings were used to fully sample the entire range.

The data reduction was performed using the *CASA* software package.[12] Standard calibration steps are carried out using a new set of *CASA* pipeline reduction procedures developed by NRAO staff. Including only the spectral windows without line emission, we then use natural weighting and multi-frequency synthesis imaging to generate the continuum images, achieving sensitivities of 5.9 μJy and 6.5 μJy beam^{-1} for BRI 1202−0725 and BRI 1335−0417, respectively. For the spectral line cubes, we also used natural weighting in the imaging, and the synthesized beamsizes are $2\farcs55 \times 1\farcs95$ (P.A. $= 2\fdg3$) and $2\farcs57 \times 1\farcs75$ (P.A. $= 7\fdg4$) in the two images. The spectral line maps are resampled to 8 MHz resolution, corresponding to velocity channel widths of 59 and 56 km s^{-1} at the redshifted frequencies of the CO $J = 2$–1 line in BRI 1202−0725 and BRI 1335−0417, while the rms per channel is 160 and 170 μJy, respectively.

3. RESULTS

Figure 1 shows the 44 GHz continuum images of the two target fields, where we also overlay contours of the 340 GHz continuum observed in BRI 1202−0725 with ALMA. The two most luminous submillimeter sources in the BRI 1202−0725 field are detected at 44 GHz, with peak flux densities of $53 \pm 6\ \mu$Jy and $24 \pm 6\ \mu$Jy for the northern and southern components, respectively. The integrated flux densities are similar to the peak values for both components, so they are unresolved. BRI 1335−0417 is also detected with a peak flux density of $40 \pm 7\ \mu$Jy, which is in agreement with the prediction by Carilli et al. (1999), who assume a thermal dust emissivity index $\beta = 1.5$. Future higher spatial resolution continuum observations will determine the size of this emission region.

From the spectral line data cubes we extract spectra of the CO $J = 2$–1 line emission at the positions of our three primary targets

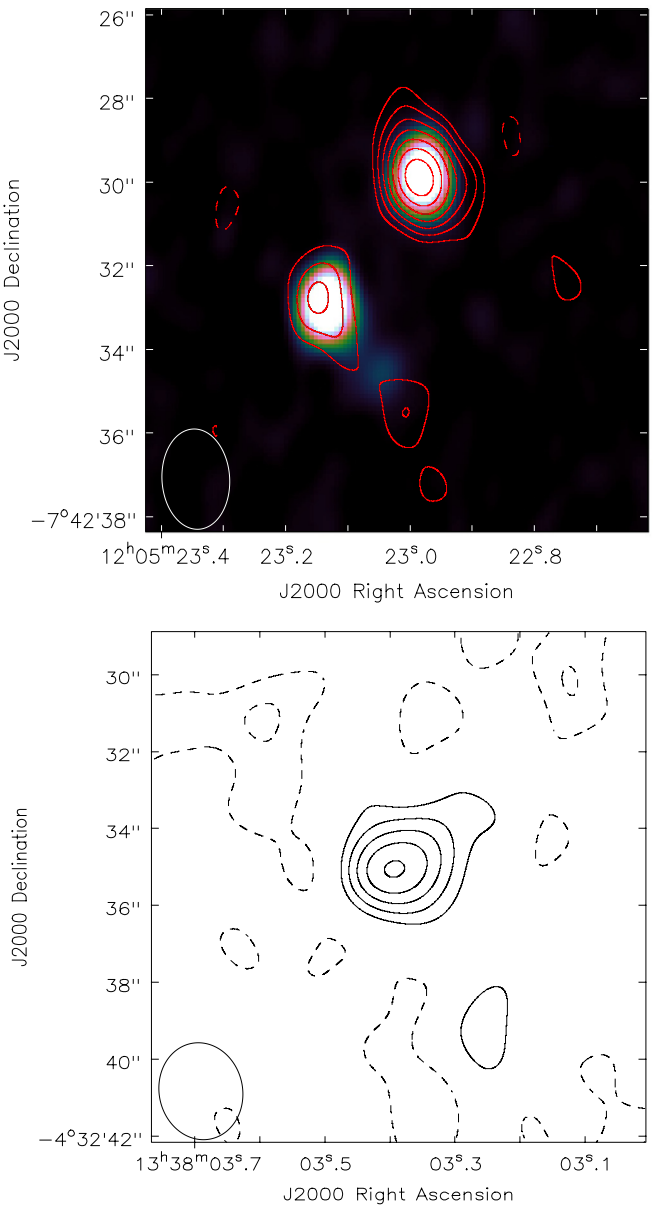

Figure 1. Top: contours of the VLA 44 GHz continuum emission from BRI 1202−0725 overlaid on the image of the 340 GHz continuum emission observed with ALMA (Wagg et al. 2012). The rms in the 340 GHz continuum image is 0.4 mJy beam^{-1}, and the synthesized beamsize is $1\farcs30 \times 0\farcs86$ (not shown). Contour intervals are (−2, 2, 3, 4, 5, 6, 7, and 8)×5.9 μJy beam^{-1}, and the synthesized beamsize is $2\farcs40 \times 1\farcs60$ (P.A. $= 3\fdg4$; bottom left). Bottom: contour map of the 44 GHz continuum emission in BRI 1335−0417 at $z = 4.4$. The beamsize is $2\farcs53 \times 1\farcs92$ (P.A. $= 6\fdg4$) and the contour levels are (−3, −2, 2, 3, 4, 5, and 6)×6.5 μJy beam^{-1}.

(A color version of this figure is available in the online journal.)

[12] http://casa.nrao.edu

Table 1
Observed Line and Continuum Properties of BRI 1202−0725 and BRI 1335−0417

Source	$S_{44\,\mathrm{GHz}}$ (μJy)	$z_{[\mathrm{CO}]}$[a]	ΔV_{FWHM}[a] (km s^{-1})	SdV (Jy km s^{-1})	$L'_{[\mathrm{CO}\,J=2-1]}$ $\times 10^{10}$ (K km s^{-1} pc^2)
BRI 1202−0725 North	51 ± 6	4.692	1108 ± 60	0.42 ± 0.04	8.7 ± 0.8
BRI 1202−0725 South	24 ± 6	4.694	352 ± 18	0.29 ± 0.02	6.0 ± 0.5
BRI 1335−0417	40 ± 7	4.406	322 ± 13	0.38 ± 0.03	7.3 ± 0.6

Note. [a] The CO $J = 2$–1 redshifts and line widths (ΔV_{FWHM}) are determined from the best-fit parameters of a Gaussian fit to the spectra.

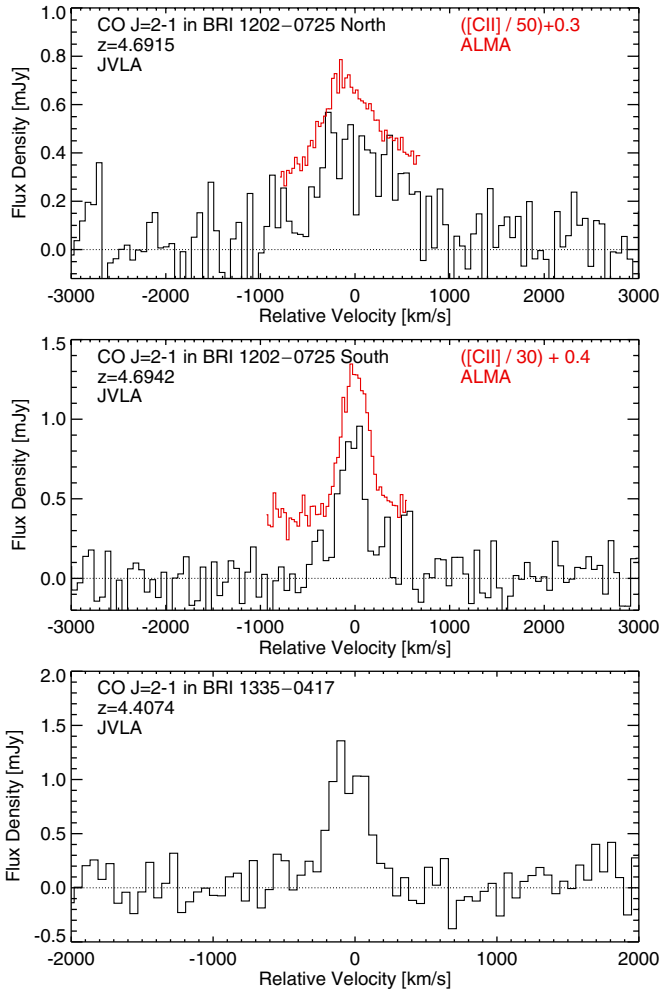

Figure 2. Top: spectra of CO $J = 2$–1 line emission in BRI 1202−0725 North and South compared with the continuum-subtracted [C II] line profiles measured by ALMA. The continuum-subtracted [C II] line emission has been scaled down and offset from zero for comparison with the CO. The velocity offsets are relative to $z = 4.6915$ and 4.6942, and the rms per 59 km s^{-1} channel is 160 μJy. Bottom: the CO $J = 2$–1 line emission detected in BRI 1335−0417 at $z = 4.4065$. The rms per 56 km s^{-1} channel is 170 μJy.

(A color version of this figure is available in the online journal.)

(Figure 2). For comparison, we show the [C II] line profiles for the BRI 1202−0725 SMG and quasar host galaxy measured from recent ALMA commissioning observations (Wagg et al. 2012; Carilli et al. 2013; Lentati et al. 2013). Table 1 gives the redshift, line widths, and integrated intensities of the CO $J = 2$–1 line emission observed here with VLA, which have been calculated assuming that the data can be described by a single Gaussian line profile. However, based on the [C II] line observations and the CO $J = 5$–4 and CO $J = 7$–6 line emission observed with the Plateau de Bure Interferometer (PdBI) by Salomé et al. (2012), the line profiles of BRI 1202−0725 North appear to be best described by two Gaussian components. The CO $J = 2$–1 redshift and line width for the quasar BRI 1202−0725 South are in excellent agreement with previous observations of [C II] and CO line emission (Omont et al. 1996; Carilli et al. 2002; Wagg et al. 2012); however, these data hint at the presence of broad wings in both sources, and more sensitive observations are needed to confirm this.

In the case of BRI 1335−0417, the CO $J = 2$–1 line profile measured here is slightly narrower than that of the previous [C II] and CO $J = 5$–4 lines detected (∼430 km s^{-1}; Guilloteau et al. 1997; Wagg et al. 2010), and also blueshifted by ∼50 km s^{-1}. The integrated intensity of the CO $J = 2$–1 line emission measured here (0.38 ± 0.03 Jy km s^{-1}) is in good agreement with the previous observations reported by Riechers et al. (2008), who measure 0.43 ± 0.02 Jy km s^{-1} using the old VLA correlator. This implies that the narrower bandwidth of past observations was wide enough to encompass the velocity width of the line, suggesting that the differences in the linewidths can be attributed to the low signal-to-noise ratio of the [C II] and CO $J = 5$–4 spectra.

4. ANALYSIS

4.1. Continuum Emission

We use archival *Herschel* SPIRE submillimeter-wavelength and lower frequency, 1.4 and 5 GHz VLA observations of our targets (project AC878) to better sample their (rest-frame) FIR through centimeter-wavelength spectral energy distributions. For BRI 1202−0725 the FIR spectral energy distribution has been observed with ALMA, PdBI, and *Herschel* SPIRE. From the level 2 pipeline-processed SPIRE maps we extract flux densities at the pixels corresponding to the 44 GHz peak position of BRI 1335−0417, measuring $S_{250\,\mu\mathrm{m}} = 33 \pm 6$ mJy, $S_{350\,\mu\mathrm{m}} = 41 \pm 5$ mJy, and $S_{500\,\mu\mathrm{m}} = 44 \pm 6$ mJy, while in the case of BRI 1202−0725 the total 350 μm flux density of both components measured in the SPIRE beam is $S_{350\,\mu\mathrm{m}} = 78 \pm 6$ mJy. Figure 3 shows the observed spectral energy distributions for BRI 1202−0725 and BRI 1335−0417.

In order to model the spectral energy distribution, we assume that the data can be described by a power-law synchrotron component dominating at frequencies below ∼30 GHz, a thermal free–free component with a power-law index of $\alpha_{\mathrm{ff}} = -0.1$, and a single-temperature graybody component that is described by a dust temperature, T_d, and emissivity index, β. Following Yun & Carilli (2002), we use the linear relationships between the total SFR and the three components describing the radio-to-FIR spectral energy distribution (Condon 1992) to obtain simultaneous constraints on all parameters in the model. The parameters we fit are therefore synchrotron spectral index, $\nu^{-\alpha}$, a scaling factor for the non-thermal synchrotron emission (f_{nth}; see Equation (13) of Yun & Carilli 2002), and finally the SFR, T_d, and β. Our fitting method is based on the principles of Bayesian

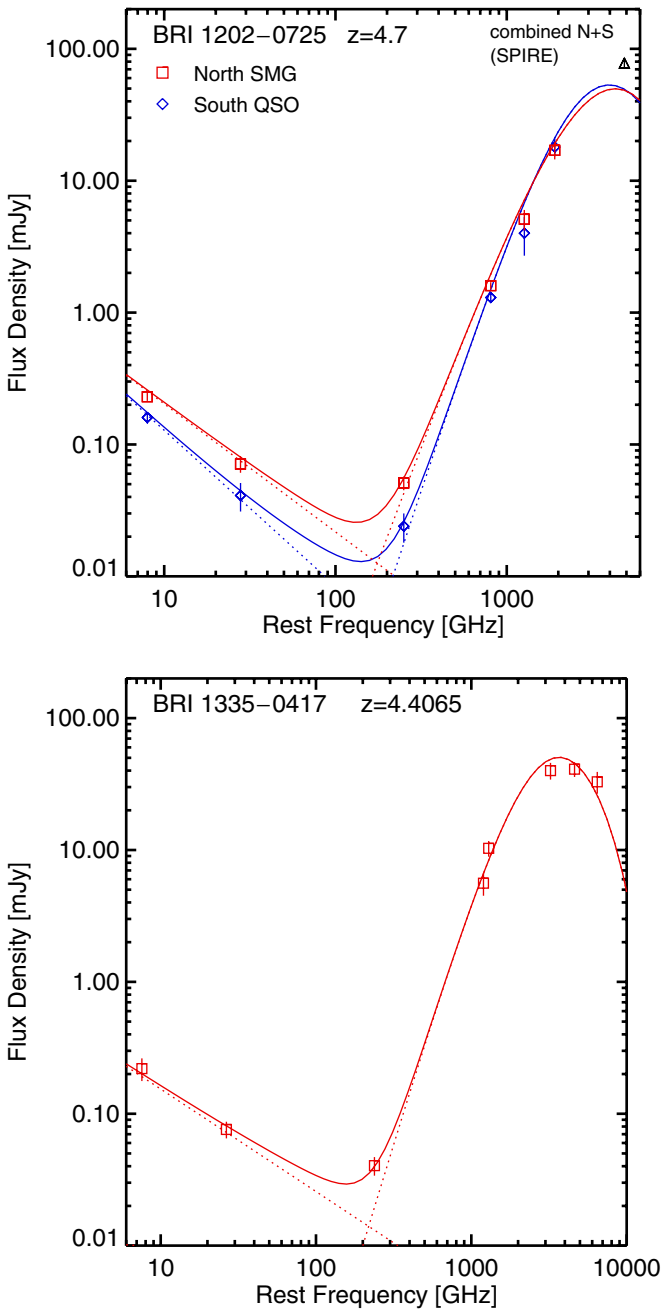

Figure 3. Top: far-infrared spectral energy distributions of BRI 1202−0725 North and South along with the best-fitting graybody, synchrotron, and thermal free–free models described in the text and parameters given in Table 2. Observed data are from Carilli et al. (2002), this work, Salomé et al. (2012), and Wagg et al. (2012). The solid curves show the best-fit models, while the dotted lines show the synchrotron and thermal dust components. The thermal free–free component of the model is not shown but does make a small contribution to the *solid* line. Bottom: the observed spectral energy distribution of BRI 1335−0417 plotted with the best-fitting model (solid line) composed of the thermal dust continuum and synchrotron emission curves (dotted lines), and only a small contribution from the thermal free–free emission. Observed data are from Carilli et al. (1999), this work, and Guilloteau et al. (1997).

(A color version of this figure is available in the online journal.)

inference, which provides a consistent approach to the estimation of a set of parameters Θ in a model or hypothesis H given the data, D. Bayes's theorem states that

$$\Pr(\Theta \mid D, H) = \frac{\Pr(D \mid \Theta, H)\Pr(\Theta \mid H)}{\Pr(D \mid H)}, \quad (1)$$

where $\Pr(\Theta \mid D, H) \equiv \Pr(\Theta)$ is the posterior probability distribution of the parameters, $\Pr(D \mid \Theta, H) \equiv L(\Theta)$ is the likelihood, $\Pr(\Theta \mid H) \equiv \pi(\Theta)$ is the prior probability distribution, and $\Pr(D \mid H) \equiv Z$ is the Bayesian evidence.

In parameter estimation, the normalizing evidence factor is usually ignored, since it is independent of the parameters Θ. Inferences are therefore obtained by taking samples from the (unnormalized) posterior using, for example, standard Markov chain Monte Carlo (MCMC) sampling methods. An alternative to MCMC is the nested sampling approach (Skilling 2004), a Monte Carlo method targeted at the efficient calculation of the evidence, which also produces posterior inferences as a by-product. In Feroz & Hobson (2008) and Feroz et al. (2009) this nested sampling framework was developed further with the introduction of the MultiNest algorithm, which provides an efficient means of sampling from posteriors that may contain multiple modes and/or large (curving) degeneracies and also calculates the evidence. We make use of the MultiNest algorithm to obtain our estimates of the posterior probability distributions for the spectral energy distribution parameters.

Naturally, the model parameters are correlated. For example, when fitting thermal dust continuum emission there are degeneracies between the emissivity index, β, and T_d (e.g., Priddey & McMahon 2001; Blain et al. 2003). These correlations can be seen in the probability density plots shown in Figure 4, and the means of the posterior parameter values are given in Table 2. Although we impose the prior that the total 350 μm emission in BRI 1202−0725 North and South should be equal to the flux density measured by SPIRE, the relative temperatures of these two components are unknown. In an attempt to overcome this, we include priors on the dust temperatures based on recent submillimeter-wavelength observations of high-redshift starburst galaxies ($T_d = 40$ K; e.g., Magnelli et al. 2012) and quasar host galaxies ($T_d = 50$ K; Beelen et al. 2006; Wang et al. 2008). However, we find that the resulting fits do a poor job of reproducing the measured 44 GHz flux densities, and so we adopt the values derived in the free-floating parameter analysis.

Evidence for thermal free–free emission has recently been observed in gravitationally lensed, FIR-luminous starburst galaxies (Thomson et al. 2012; Aravena et al. 2013). The models provide an estimate of the contribution from such free–free emission to the observed 44 GHz continuum emission in our targets. Based on the fitting analysis, the main contribution to the 44 GHz flux density in each source is thermal dust continuum emission. In the case of BRI 1335−0417, that contribution is 54%, with 30% coming from synchrotron emission and only 16% from thermal free–free emission. In the case of the SMG BRI 1202−0725 North, the thermal dust emission contribution from our model fit is 75%, while 17% and 8% come from synchrotron and free–free emission, respectively. The model fit to the spectral energy distribution of the quasar BRI 1202−0725 South has a 67% contribution to the 44 GHz flux density from thermal dust emission, while only 12% comes from synchrotron emission and 21% is found to come from free–free emission. Although it is not considered in our models, another possibility is that the 44 GHz emission arises from a flat-spectrum AGN embedded in the starburst host galaxies; however, higher resolution imaging is needed before we can determine the likelihood of this.

4.2. CO $J = 2$–1 Line Emission

Following the definition of line luminosity given by Solomon et al. (1992), we calculate the line luminosities to be

Table 2
Best-fit Spectral Energy Distribution Model Parameters for BRI 1202−0725 and BRI 1335−0417

Source	SFR ($M_\odot$ yr^{-1})	α	log $f_{\rm nth}$	T_d (K)	β
BRI 1202−0725 North	3508 ± 1990	0.97 ± 0.13	0.88 ± 0.26	67.8 ± 17.5	1.54 ± 0.19
BRI 1202−0725 South	4411 ± 2141	1.17 ± 0.17	0.79 ± 0.26	63.7 ± 15.6	2.04 ± 0.22
BRI 1335−0417	5040 ± 1304	0.91 ± 0.18	0.52 ± 0.27	58.3 ± 4.5	1.89 ± 0.23

Note. Values quoted are the mean and 1σ uncertainty.

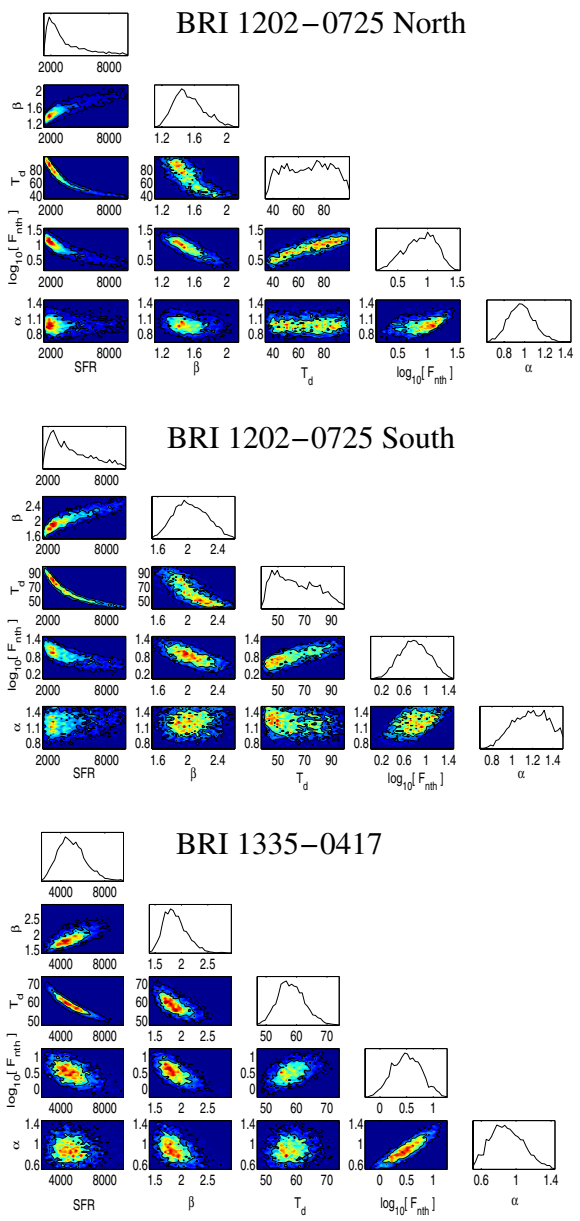

Figure 4. Parameter probability density plots for our three targets resulting from the MultiNest Bayesian fitting analysis. Each plot shows how the fit parameters are correlated when fitting the model described in the text to the observed data. The curves plotted at the top of each column indicate the probability distribution for the parameter in the label at the bottom. The mean of the posterior values and 1σ confidence intervals are given in Table 2.

(A color version of this figure is available in the online journal.)

$L'_{\rm CO} = (8.7 \pm 0.8) \times 10^{10}$ K km s^{-1} pc^2 and $L'_{\rm CO} = (6.0 \pm 0.5) \times 10^{10}$ K km s^{-1} pc^2 for BRI 1202−0725 North and South, respectively, and $L'_{\rm CO} = (7.3 \pm 0.6) \times 10^{10}$ K km s^{-1} for BRI 1335−0417. For BRI 1202−0725, these luminosities are in excellent agreement with previous lower spectral resolution observations with VLA (Carilli et al. 2002), as well as with the high-J CO lines measured by Omont et al. (1996) and Salomé et al. (2012), and support the claim that the line emission is thermalized. This is also the case for BRI 1335−0417, for which the CO $J = 5$–4 line luminosity, $L'_{\rm CO} = (8.5 \pm 0.9) \times 10^{10}$ K km s^{-1} pc^2, measured by Guilloteau et al. (1997) is similar to what we measure in CO $J = 2$–1.

ALMA observations reveal [C II] line emission in the two Lyα emitters at $z \sim 4.7$ associated with the BRI 1202−0725 system (Carilli et al. 2013). We search the Q-band spectral line data cubes at the positions of Lyα-1 and Lyα-2 and the expected frequencies of redshifted CO $J = 2$–1, but this emission is undetected. Assuming Gaussian line profiles, we set 3σ upper limits to the line luminosities, $L'_{\rm CO} < 4.8 \times 10^9$ K km s^{-1} pc^2 and $L'_{\rm CO} < 1.2 \times 10^{10}$ K km s^{-1} pc^2 for Lyα-1 and Lyα-2 assuming FWHM linewidths of 56 and 338 km s^{-1}.

5. DISCUSSION

Although the uncertainties are large, the SFRs estimated for the three targets are similar to previous estimates derived from the FIR luminosities (e.g., Wagg et al. 2010; Salomé et al. 2012; Carniani et al. 2013). The FIR emission model fit to the SMG BRI 1202−0725 North favors an emissivity index of $\beta \sim 1.5$, while the quasars BRI 1202−0725 South and BRI 1335−0417 appear to have values closer to $\beta \sim 2.0$. Both of these values are similar to what has been measured in 60 μm selected galaxies in the nearby universe (e.g., Dunne et al. 2000). More recent studies of the full FIR through submillimeter-wavelength emission in normal star-forming galaxies from the KINGFISH sample show that nearby galaxies can exhibit a broad range in emissivity indices, $\beta \sim 0.8$–2.5 (Galametz et al. 2012). Our measured values are therefore not unusual. If free–free emission does not contribute significantly to the 44 GHz emission observed in BRI 1202−0725 North, then these data suggest that the cold dust mass is a factor of ∼2.5 higher than that in the quasar BRI 1202−0725 South.

In all three sources, the contribution from thermal free–free emission to the rest-frame 250 GHz continuum is $\lesssim$20%. Free–free emission typically contributes less than 10% of the 230 GHz continuum emission observed in normal, nearby galaxies (e.g., Albrecht et al. 2007), and so our results are consistent with what is observed in these more quiescent star-forming galaxies. Strong free–free emission has been detected in lensed SMGs (Aravena et al. 2013), and the SFRs estimated are in good agreement with those estimated from the FIR luminosities.

Our measured CO $J = 2$–1 line luminosities are in good agreement with previous observations of both the low- and high-J CO emission observed in these objects (Guilloteau et al. 1997; Carilli et al. 2002; Riechers et al. 2006, 2008). The luminosities imply cold molecular gas masses ∼10^{11} $M_\odot$ assuming

the recently measured value $\alpha_{CO} = 0.6\,M_{\odot}\,(\mathrm{K\,km\,s^{-1}\,pc^2})^{-1}$ for the CO-to-H_2 conversion factor in ultraluminous infrared galaxies (ULIRGs; Papadopoulos et al. 2012), similar to the original value of Downes & Solomon (1998). However, we note that this factor can be uncertain by ~8 for ULIRGs. A recent analysis of the [C II] line emission observed in BRI 1202−0725 infers dynamical masses for the quasar and SMG based on the kinematic properties of the gas (Carniani et al. 2013). They calculate dynamical masses of $M_{\mathrm{dyn}} \sim 4 \times 10^{10}\,M_{\odot}$ and $\sim 6 \times 10^{10}\,M_{\odot}$ for the quasar and SMG, respectively, implying very high molecular gas mass fractions of ~80%–90%. Such high gas fractions are inferred for some local ULIRGs (e.g., Papadopoulos et al. 2012). Planned subarcsecond imaging of this cold molecular gas in these targets would be complemented by higher resolution imaging of the (rest-frame) FIR continuum and [C II] line emission with ALMA in order to infer the ionizing radiation field and gas density on kpc scales.

6. SUMMARY

We present VLA observations of redshifted CO $J = 2$–1 line and thermal dust continuum emission in high-redshift quasar host galaxies, observing BRI 1202−0725 and BRI 1335−0417. The luminosities measured in the CO $J = 2$–1 line detected in all three targets are similar to previous observations of CO $J = 5$–4 line emission, implying that the gas kinetic temperature is close to the excitation temperature. The observations reveal strong (rest-frame) 250 GHz continuum emission associated with all three FIR luminous galaxies, with stronger emission observed in the two starburst galaxies than the quasar BRI 1202−0725 South. Although synchrotron and thermal free–free likely contribute to some of this emission, we interpret the remainder as due to thermal dust emission. Future observations at frequencies between 10 and 40 GHz will allow us to better constrain the relative importance of the three processes.

We thank Maud Galametz, Rob Kennicutt, Thomas Greve, and Padelis Papadopoulos for helpful discussions, and the anonymous referee for their comments on the submitted manuscript. This work was co-funded under the Marie Curie Actions of the European Commission (FP7-COFUND). We thank all those involved in the VLA project for making these observations possible (project code 13A-012). This paper makes use of the following ALMA data: ADS/JAO.ALMA#2011.0.00006.SV. ALMA is a partnership of ESO (representing its member states), NSF (USA), and NINS (Japan), together with NRC (Canada) and NSC and ASIAA (Taiwan), in cooperation with the Republic of Chile. The Joint ALMA Observatory is operated by ESO, AUI/NRAO, and NAOJ. The National Radio Astronomy Observatory is a facility of the National Science Foundation operated under cooperative agreement by Associated Universities, Inc.

REFERENCES

Albrecht, M., Krügel, E., & Chini, R. 2007, A&A, 462, 575
Aravena, M., Murphy, E. J., Aguirre, J. E., et al. 2013, MNRAS, 433, 498
Beelen, A., Cox, P., Benford, D. J., et al. 2006, ApJ, 642, 694
Benford, D. J., Cox, P., Omont, A., Phillips, T. G., & McMahon, R. G. 1999, ApJL, 518, L65
Blain, A. W., Barnard, V. E., & Chapman, S. C. 2003, MNRAS, 338, 733
Carilli, C. L., Kohno, K., Kawabe, R., et al. 2002, AJ, 123, 1838
Carilli, C. L., Menten, K. M., & Yun, M. S. 1999, ApJL, 521, L25
Carilli, C. L., Riechers, D., Walter, F., et al. 2013, ApJ, 763, 120
Carilli, C. L., & Walter, F. 2013, ARA&A, 51, 105
Carniani, S., Marconi, A., Biggs, A., et al. 2013, A&A, 559, A29
Condon, J. J. 1992, ARA&A, 30, 575
Downes, D., & Solomon, P. M. 1998, ApJ, 507, 615
Dunne, L., Eales, S., Edmunds, M., et al. 2000, MNRAS, 315, 115
Feroz, F., & Hobson, M. P. 2008, MNRAS, 384, 449
Feroz, F., Hobson, M. P., & Bridges, M. 2009, MNRAS, 398, 1601
Galametz, M., Kennicutt, R. C., Albrecht, M., et al. 2012, MNRAS, 425, 763
Guilloteau, S., Omont, A., McMahon, R. G., Cox, P., & Petitjean, P. 1997, A&A, 328, L1
Hu, E., McMahon, R. G., & Egami, E. 1996, ApJL, 459, L53
Iono, D., Yun, M. S., Elvis, M., et al. 2006, ApJL, 645, L97
Irwin, M., McMahon, R. G., & Hazard, C. 1991, in ASP Conf. Ser. 21, The Space Distribution of Quasars, ed. D. Crampton (San Francisco, CA: ASP), 117
Ivison, R. J., Papadopoulos, P. P., Smail, I., et al. 2011, MNRAS, 412, 1913
Ivison, R. J., Swinbank, A. M., Swinyard, B., et al. 2010, A&A, 518, L35
Lentati, L., Carilli, C., Alexander, P., et al. 2013, MNRAS, 430, 2454
Magnelli, B., Lutz, D., Santini, P., et al. 2012, A&A, 539, A155
Maiolino, R., Cox, P., Caselli, P., et al. 2005, A&A, 440, L51
Ohta, K., Yamada, T., Nakanishi, K., et al. 1996, Natur, 382, 426
Omont, A., Petitjean, P., Guilloteau, S., et al. 1996, Natur, 382, 428
Papadopoulos, P. P., van der Werf, P., Xilouris, E., Isaak, K. G., & Gao, Y. 2012, ApJ, 751, 10
Priddey, R. S., & McMahon, R. G. 2001, MNRAS, 324, L17
Riechers, D. A., Carilli, L. C., Walter, F., et al. 2011, ApJL, 733, L11
Riechers, D. A., Walter, F., Carilli, C. L., Bertoldi, F., & Momjian, E. 2008, ApJL, 686, L9
Riechers, D. A., Walter, F., Carilli, C. L., et al. 2006, ApJ, 650, 604
Salomé, P., Guélin, M., Downes, D., et al. 2012, A&A, 545, A57
Skilling, J. 2004, in AIP Conf. Proc. 735, Bayesian Inference and Maximum Entropy Methods in Science and Engineering (Melville, NY: AIP), 395
Solomon, P. M., Downes, D., & Radford, S. J. E. 1992, ApJL, 398, L29
Spergel, D. N., Bean, R., Doré, O., et al. 2007, ApJS, 170, 377
Stacey, G. J., Geis, N., Genzel, R., et al. 1991, ApJ, 373, 423
Stacey, G. J., Hailey-Dunsheath, S., Ferkinhoff, C., et al. 2010, ApJ, 724, 957
Storrie-Lombardi, L. J., McMahon, R. G., Irwin, M. J., & Hazard, C. 1996, ApJ, 468, 121
Thomson, A. P., Ivison, R. J., Smail, I., et al. 2012, MNRAS, 425, 2203
Venemans, B. P., McMahon, R. G., Walter, F., et al. 2012, ApJL, 751, L25
Wagg, J., Carilli, C. L., Wilner, D. J., et al. 2010, A&A, 519, L1
Wagg, J., Wiklind, T., Carilli, C. L., et al. 2012, ApJL, 752, L30
Wang, R., Wagg, J., Carilli, C. L., et al. 2008, AJ, 135, 1201
Wang, R., Wagg, J., Carilli, C. L., et al. 2013, ApJ, 773, 44
Yun, M. S., & Carilli, C. L. 2002, ApJ, 568, 88
Yun, M. S., Carilli, C. L., Kawabe, R., et al. 2000, ApJ, 528, 171